J Sol-Gel Sci Technol
DOI 10.1007/s10971-012-2952-y

Physicochemical properties of V^{5+} doped $LiCoPO_4$ as cathode materials for Li-ion batteries

A. Rajalakshmi · V. D. Nithya · K. Karthikeyan · C. Sanjeeviraja · Y. S. Lee · R. Kalai Selvan

Received: 5 July 2012 / Accepted: 24 December 2012

Abstract Phase pure olivine type V^{5+} doped and un-doped $LiCoPO_4$ ($LiCo_{1-x}V_xPO_4$ & $LiCoP_{1-x}V_xO_4$; x = 0.02, 0.04 and 0.06) were synthesized by combustion method. Compound formation temperature and thermal stability of the materials were studied through thermal analysis. X-ray diffraction pattern shows the prepared material possesses an orthorhombic structure with *Pnmb* space group. Further the functional group and vibrational analysis were carried out by Fourier Transform Infra-red and Raman spectroscopy techniques. The Scanning Electron Micrographs depicts the irregular shaped morphology with particle agglomeration of the pristine and doped $LiCoPO_4$ materials. The structural variation on addition of dopant on both sites Co^{2+} & P^{5+} were revealed from XPS spectra. The electrochemical aspects of these materials were investigated by cyclic voltammetry studies in conjunction with electrochemical impedance spectroscopy and chronoamperommetry measurements to understand the redox reactions and their capacity contribution at higher voltages. The EIS analysis shows that the conductance value was decreased for the vanadium doped samples for both the Co site and P site, which infers that the V^{5+} addition doesn't make any significant enhancement in the electrochemical performance of the $LiCoPO_4$.

Keywords $LiCoPO_4$ · Cathode materials · Li-ion batteries · X-Ray diffraction

1 Introduction

The most surprising feature of today's battery industry continues to be the recent development and growth of Li-ion battery technology. Because of its superior energy density, the Li-ion battery is now the battery of choice in various mobile products and applications such as uninterruptible power supply (UPS) systems, photovoltaic power generation, energy recovery systems in industrial machinery, and transportation systems. However research is still focused to achieve a good class of electrode materials mainly a cathode material for high voltage cells. A series of cathode materials have been identified including TiS_2, $LiCoO_2$, & $LiMn_2O_4$ [1–3] and studied their detailed performances. The commercialized cathode material is layered structure $LiCoO_2$ with a flat voltage of 3.9 V. It is prevented from wide applications because it possess drawbacks like not stable when overcharged, material degradation can occur on repeated charging, the formation of CoO_2 phase can shear the electrode surface, after the full delithiation stoichiometric $LiCoO_2$ can be difficult to obtain and costly. Hence heat treatment is necessary to control the phase content to improve the performance.

Recently a new set of olivine type phosphate materials $LiMPO_4$ (where M = Fe, Mn, Co & Ni) were studied as advanced cathode materials for lithium-ion batteries because these lithium metal phosphates possess an attracting electrochemical and thermal stability with high

A. Rajalakshmi · V. D. Nithya · R. Kalai Selvan (✉)
Solid State Ionics and Energy Devices Laboratory, Department of Physics, Bharathiar University, Coimbatore 641 046, India
e-mail: selvankram@buc.edu.in

K. Karthikeyan · Y. S. Lee (✉)
Faculty of Applied Chemical Engineering, Chonnam National University, Gwang-ju 500-757, Korea
e-mail: leeys@chonnam.ac.kr

C. Sanjeeviraja
School of Physics, Alagappa University, Karaikudi 630 003, India

Published online: 08 January 2013

theoretical capacity of 170 mAh g^{-1}, which was studied by Padhi et al. [4] and later works by Martha et al. [5, 6]. Among the olivine materials, recent works are focused on $LiCoPO_4$ because of its high operating voltage (4.8 V). The material $LiCoPO_4$ crystallizes in the olivine structure usually has orthorhombic symmetry and the presence of polyanionic group (PO_4^{3-}) in the compound with strong covalent bonds gives a structural stability during lithium insertion and extraction. This makes the compound as a potential cathode material for Li-ion battery. The electrochemical performance of $LiCoPO_4$ with specific capacity of 100 mAh g^{-1} was first revealed by Okada et al. [7]. After that, many research groups were tried to improve the practical electrochemical performance of $LiCoPO_4$ using different synthesis methods like polymer precursor [8], solid state reaction [9, 10], rheological phase method [11] hydrothermal [13], high energy milling [14], and sol–gel methods [15]. It was found that the electrochemical performance was greatly influenced by synthesis techniques which indirectly driven the particle size [14] and morphology [8]. Though $LiCoPO_4$ possesses high voltage, the material suffers from poor electrical conduction which may lead to irreversibility and poor storage capacity. It is known that the reversibility of the electrochemical system is mainly dependent on electrical conductivity and particle morphology.

In recent years, many approaches were employed to improve the electrical conduction of $LiCoPO_4$. One such approach is carbon coating on $LiCoPO_4$ which leads to a better electrochemical performance with the capacity of 110 mAh g^{-1} [16]. Secondly, by means of suitable metal ion doping, for example Fe^{2+}, V^{5+} and Mn^{2+}, in the Co^{2+} site with carbon coating [17–22], and doping Mn^{2+}, Mg^{2+}, and Ni^{2+} at the metal site without carbon coating [23–25] were attempted. It was shown that better electrochemical performance could be achieved by increasing the electrical conduction from 10^{-9} to 10^{-7} Scm^{-1}. Further the electrochemical performance of the material were enhanced by surface modification of Fe doped $LiCoPO_4$ by $LiFePO_4$ [26]. Similarly, doping $LiCoPO_4$ with Cr & Cu at Li^+ and Co^+ site were also tried to improve the conductivity of the material [27].

In the present work, for the first time, we tried to study the effect of doping on pristine $LiCoPO_4$ at two different elemental sites i.e. Co^{2+} & P^{5+} sites, with vanadium V^{5+} ($LiCo_{1-x}V_xPO_4$, $LiCoP_{1-x}V_xO_4$) at different concentrations x = 0.02, 0.04 and 0.06 without carbon coating. The structural, electrical and electrochemical properties of the doped materials in comparison with the pristine $LiCoPO_4$ were studied. Vanadium has been chosen as a dopant because the pentavalent ions in the host lattice might increase the carrier concentrations to enhance the electrical conduction and there by improves the electrochemical performance.

2 Experimental methods and materials

$LiCoPO_4$, $LiCo_{1-x}V_xPO_4$, & $LiCoP_{1-x}V_xO_4$ were synthesized by combustion method. Combustion method is a simple and fast synthetic approach to prepare high purity nanomaterials [12]. Moreover, this is an economically viable technique which does not require enormous external energy. Stoichiometric quantities of starting materials LiCl, $Co(NO_3)_2.6H_2O$, & $NH_4H_2PO_4$ were dissolved with suitable amount of double distilled water and mixed thoroughly by constant stirring to form a homogeneous mixture. Then stoichiometric amount of urea [$(NH_2)_2CO$] was added as a fuel. Moreover, the reaction was done with the pH value of 10 which was adjusted by adding small amount of ammonia solution into the reaction mixture. The mixture was dried by heating at 100 °C with continuous stirring to get a sticky paste and then dried samples were heat treated at about 400 °C at which the materials get ignited with the rapid evolution of a large volume of dense fumes of gaseous products, resulting in a final foamy powder which was later calcined in air atmosphere at 800 °C for 5 h. The same procedure was repeated for the doped samples by taking NH_4VO_3 as a source for vanadium.

The reaction mechanism for the formation of $LiCoPO_4$ by combustion synthesis is given in Scheme 1. The reaction among the starting precursor proceeds may be as follows. First, the Lithium chloride (LiCl) reacts with Ammonium dihydrogen phosphate ($NH_4H_2PO_4$) to form Ammonium chloride (NH_4Cl) and Lithium dihydrogen phosphate (LiH_2PO_4) [Step 1]. Next the Cobalt nitrate reacts with urea to form di nitrato uryl cobalt (II) [Step 2]. The products of Step 1 & 2, Lithium dihydrogen phosphate and dinitrato uryl cobalt (II) reacts to form an intermediate compound called Lithium diphosphato uryl cobaltate (III) [Step 3] which when heated to form the final product $LiCoPO_4$ along with some volatile compounds such as NH_3, HCl, HNO_3, CO and PO.

Thermal stability of green samples before calcination was conducted by thermogravimetry and differential thermal analysis technique (Q600 DT) TG/DTA in the temperature range 40–800 °C. The obtained samples were subjected to various characterization techniques to investigate its physical & electrochemical properties. The crystalline phase and structure of the prepared materials were studied from X-ray diffraction technique (Bruker D8, Advance) using CuKα radiation (λ = 1.5406 Å). The functional group analysis of the compounds were taken and verified by Fourier transform infra-red spectroscopy FTIR technique (Nicolet Avatar Model) in the frequency range of 400–2,000 cm^{-1} and Raman Analysis (Lab Ram HR 800) were carried out with laser raman confocal microprobe using He–Ne laser as excitation source with wavelength of λ = 633 nm in the frequency range 100–1,100 cm^{-1}. The

Scheme 1 Reaction mechanism for the formation of $LiCoPO_4$ by combustion synthesis

Step 1:

Step 2:

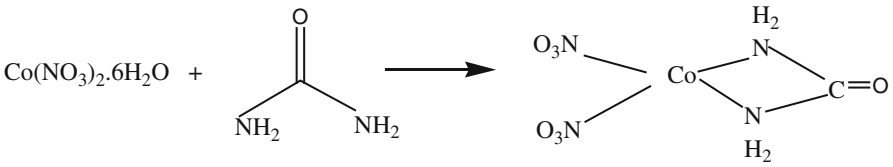

Step 3:

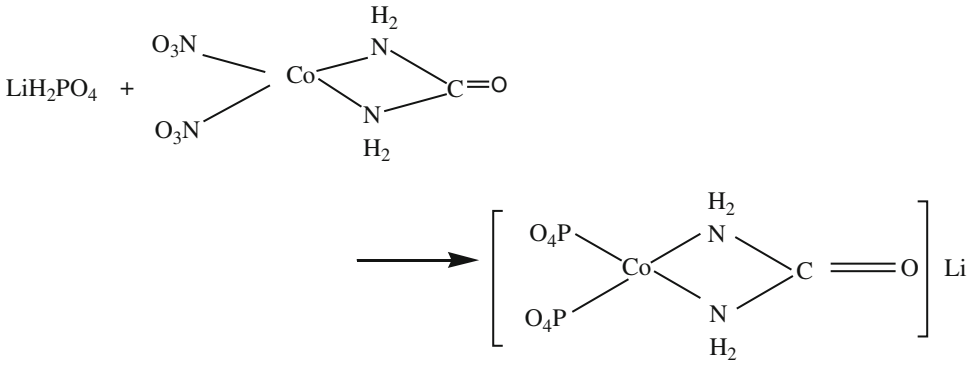

Step 4:

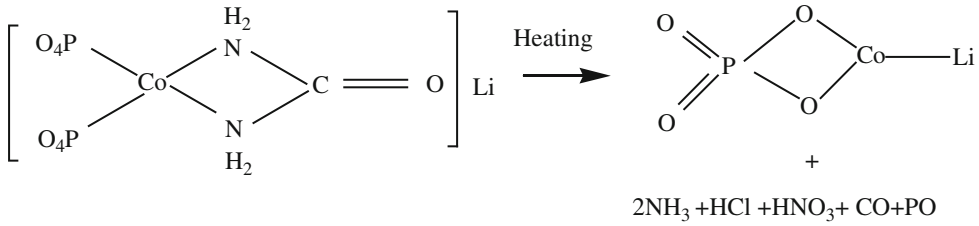

morphology of the materials was viewed using high resolution scanning electron microscopy (HRSEM FEI Quanta FEG 200) analysis. Further the structural variation on addition of dopant Vanadium at Co^{2+} & P^{5+} sites were verified with the chemical binding energy values obtained from high resolution O 1s, P 2p, Co 2p XPS Spectra. The X-ray photoelectron spectrometry was obtained by multilab 2000, UK with a monochromator using Al Kα radiation of hν 1486.6 eV.

The electrochemical impedance spectroscopy (EIS) and cyclic Voltammetry studies (CV) were performed using a Bio-Logic electrochemical work station (SP-150, Biologic, France). The galvanostatic charge/discharge testing was done using a battery tester WBCS 3000, Won-A-Tech, Korea. CV measurements were carried out using Li metal as counter and reference electrodes and the measurements were carried out in the potential range of 2.8–5.5 V at the scan rate of 0.2 mVs^{-1} with 1 M $LiPF_6$ (1:1 EC: DMC v/v) electrolyte. The charge–discharge studies were obtained using a CR2032 coin-type cell between 3.5 and 5.5 V with 0.1 mA cm^{-2} current density at room temperature. The cathode was fabricated with 20 mg of active material, 3 mg of ketzen black and 3 mg of conductive binder (2 mg of Teflonized acetylene black (TAB) and 1 mg of graphite). It was pressed on 200 mm^2 stainless steel mesh which was used as the current collector under a pressure of 300 kg cm^{-2} and dried at 130 °C for 5 h in an oven. The test cells were prepared in Ar-filled glove box with the synthesized materials as cathode and lithium metal anode, separated by porous polypropylene film (Celgard 3401).

3 Results and discussion

3.1 Thermal analysis

The thermal stability of the material is studied by using TG/DTA analysis. The behavior of the material is studied

by heating the material from room temperature to 800 °C at a heating rate of 10 °C min^{-1}. The TG/DTA curves of as-prepared $LiCoPO_4$, and doped samples of $LiCo_{1-x}V_xPO_4$ and $LiCoP_{1-x}V_xO_4$ with different concentration (x = 0.02, 0.04, 0.06) are shown in Fig. 1a, b respectively. It can be seen that the TGA curve of pristine $LiCoPO_4$ shows three different weight losses from 40 to 400 °C. The first weight loss observed in the range of 40–116 °C corresponds to the evaporation of moisture content present in the sample. The second weight loss in the range of 116–230 °C was due to the decomposition of other organic compounds remaining as the residues as the combustion product due to the addition of fuel. The evaporation of volatile gases takes place within the range of 400 °C. Above 400 °C, the compound formation occurs which is shown in the corresponding DTA curve of Fig. 1b. An exothermic peak was observed around 415 °C, which shows a formation of complex compound and was completed at 600 °C. There was no significant weight loss observed between 600 and 800 °C indicating that the compounds are stable at high temperature [15], with only 4 % loss of initial weight.

Similar results were observed for the doped samples but with small changes in the weight loss ranges (Table 1). As it is seen from the table, the onset of weight loss in temperatures for the doped material are shifted to higher values especially vanadium doped samples compared with the parent $LiCoPO_4$. The weight loss percentages of the cobalt site doped compounds $LiCo_{1-x}V_xPO_4$ are only about 1–2 % which is smaller than the parent material. $LiCoP_{0.98}V_{0.02}O_4$, $LiCoP_{0.96}V_{0.04}O_4$ and $LiCoP_{0.94}V_{0.06}O_4$ shows 4–6, 2–3, 3–5 % loss of the initial weight which is higher than the weight loss percentage of the parent. It is unclear about the anomalous thermal behavior observed for the vanadium doped samples at Co site and P site. However, all the materials (both doped and undoped $LiCoPO_4$) reach a thermal stability at 600–800 °C. Based on this result, the calcination temperatures of the as prepared samples are set as 800 °C for 5 h to obtain pure phase samples.

3.2 X-ray diffraction studies

Figure 2 shows the XRD pattern of doped and undoped $LiCoPO_4$ cathode materials recorded in the range of 10–60°. No other impurity peaks were observed in the XRD pattern which indicates that the formed compounds are in single phase. The lattice parameters were calculated using CELREF software attributed to an orthorhombic structure with *Pnmb* space group which is in good agreement with the standard JCPDS card no. 32-0552. The diffraction peaks of doped materials were similar to that of the pristine $LiCoPO_4$ without any impurity peaks. The corresponding lattice parameters, cell volume, lattice density and crystallite size are given in Table 1. The crystallite

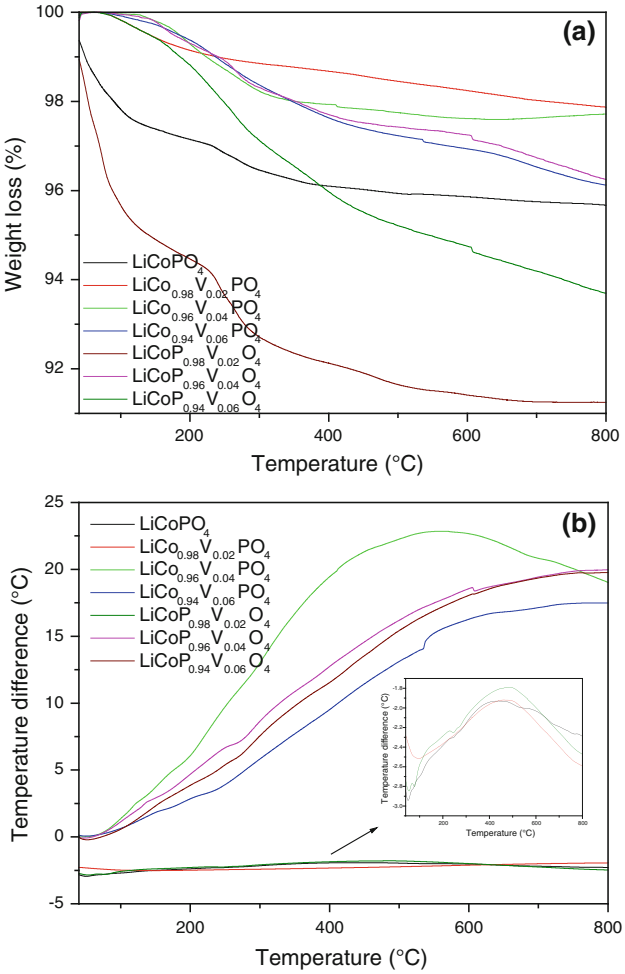

Fig. 1 **a** TG curves and **b** DTA curves of parent and doped green samples (Color figure online)

sizes were calculated for the high intensity planes using Scherer formula and are shown in Table 1. The crystallite sizes calculated from different miller indices were in the range of 80–120 nm for both doped and un-doped $LiCoPO_4$. No sequence variation in sizes were observed for doped $LiCoPO_4$ compared with the parent material. From the XRD data, it was observed that there was a change in the lattice parameters and the cell volume due to the effect of dopant. When comparing the parameters between the doped samples of different site with the parent $LiCoPO_4$ material individually, small changes were noticed in the lattice parameters which might be due to the difference in ionic radii of the doped vanadium. It is observed from the table that in the case of $LiCo_{1-x}V_xPO_4$ the overall cell volume gets reduced because the ionic radii of vanadium (0.54Å) is small when compared to cobalt (0.75Å), whereas in the case of $LiCoP_{1-x}V_xO_4$ no appreciable changes in the cell volume were observed, since ionic radii of phosphorous is (0.38Å) smaller than the vanadium [23]. Similar behavior of reduction in cell volume on the

Table 1 Thermal studies and structural parameters of doped and un-doped $LiCoPO_4$

Compounds	TGA (weight loss) °C		Lattice parameters (Å)			Cell volume $(Å)^3$	Lattice density (g cm^{-3})	Crystallite size for the corresponding (hkl) miller plane (nm)		
	1st	2nd	a	b	c			(020)	(111)	(200)
$LiCoPO_4$	40–116	116–230	5.9026	10.1758	4.6766	280.8933	3.802	89	60	79
$LiCo_{0.98}V_{0.02}PO_4$	42–118	118–229	5.903	10.1694	4.6803	280.9733	3.801	110	78	75
$LiCo_{0.96}V_{0.04}PO_4$	46–147	147–209	5.8990	10.1665	4.6742	280.3226	3.810	196	91	91
$LiCo_{0.94}V_{0.06}PO_4$	44–171	171–230	5.8926	10.1552	4.6689	279.3879	3.823	98	55	81
$LiCoP_{0.98}V_{0.02}O_4$	43–117	117–222	5.8901	10.1616	4.6664	279.2991	3.801	116	73	111
$LiCoP_{0.96}V_{0.04}O_4$	39–138	138–214	5.8978	10.1666	4.6762	280.3868	3.810	72	60	90
$LiCoP_{0.94}V_{0.06}O_4$	40–149	149–227	5.8904	10.1658	4.6782	280.1328	3.813	126	59	78

addition of vanadium in the Co site was observed for $LiCo_{0.9}V_{0.1}PO_4$/C [20]. Therefore, it was expected that the doping in cobalt site material would be different from the phosphate site doped material but the addition of vanadium does not show any appreciable change in the structure of the compound even at high dopant concentration. This shows that the minimum concentration levels might not perturb the host lattice significantly.

3.3 Morphological analysis

The morphological analysis of the synthesized materials was analyzed by High resolution scanning electron microscopic (HRSEM) images. Figure 3 shows the HRSEM image of pristine $LiCoPO_4$, $LiCo_{1-x}V_xPO_4$ and $LiCoP_{1-x}V_xO_4$ ($x = 0.02, 0.04, 0.06$). It is seen from the image (Fig. 3a), the pristine $LiCoPO_4$ compound contains some irregularly shaped particles with sizes in the range of 1–2 µm. The distribution of the particle is not uniform and contains randomly distributed micro particles. It is observed that in the case of vanadium doped samples in Co site, the particle size initially gets decreases for lower amount of dopant addition i.e. $x = 0.02$. When the amount of dopant gets increased the smaller particles tends to get agglomerated into slightly larger micro crystals. It is also noticed that, the particle agglomeration is enhanced for higher amount of vanadium addition ($x = 0.06$) and the particle size gets increased in the doped samples. In case of P site doped materials, slightly larger sized particles were observed compared with the parent $LiCoPO_4$ material and are agglomerated. The observed particle agglomeration might be due to the high calcination temperature employed for material preparation. Similar type of irregular and agglomerated morphology was reported previously [8, 16, 36]. Additionally, the compositional analysis of the parent $LiCoPO_4$ was done by Energy Dispersive Analysis of X-Ray (EDAX) analysis and the corresponding EDAX spectrum of $LiCoPO_4$ was given in Fig. 3h. This spectrum shows the characteristics peaks of Co, P and O present in the sample and no other impurity peaks were detected confirming the phase purity of the material.

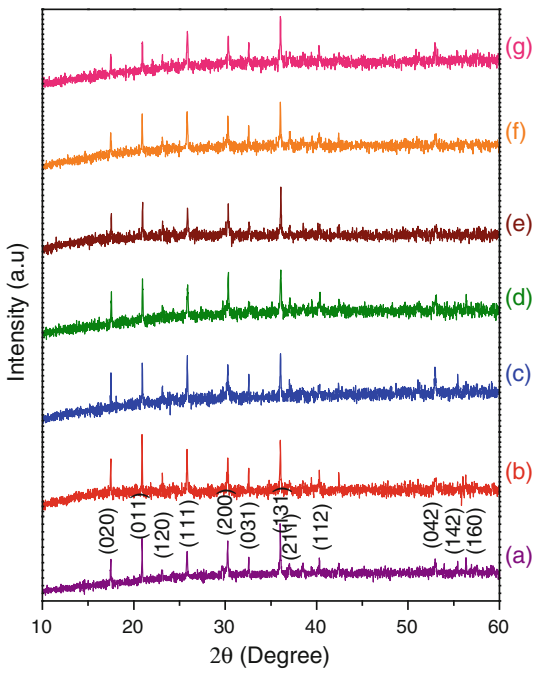

Fig. 2 XRD pattern of (*a*) $LiCoPO_4$, (*b*) $LiCo_{0.98}V_{0.02}PO_4$, (*c*) $LiCo_{0.96}V_{0.04}PO_4$, (*d*) $LiCo_{0.94}V_{0.06}PO_4$, (*e*) $LiCoP_{0.98}V_{0.02}O_4$, (*f*) $LiCoP_{0.96}V_{0.04}O_4$ and (*g*) $LiCoP_{0.94}V_{0.06}O_4$

3.4 FT-IR analysis

The FT-IR spectrum of pristine and vanadium doped samples of $LiCoPO_4$ are shown in Fig. 4. The curve shows four fundamental vibrations (ν_1–ν_4) which was attributed to the stretching and bending modes of polyanion PO_4^{3-} and the small splitting is due to the inductive effect of M–O octahedral sites [28]. The obtained spectra were dominated by the stretching mode (O–P–O) of the PO_4^{3-} group. Because it is known that the fundamental vibrational frequency of olivine compounds arise from the polyanion

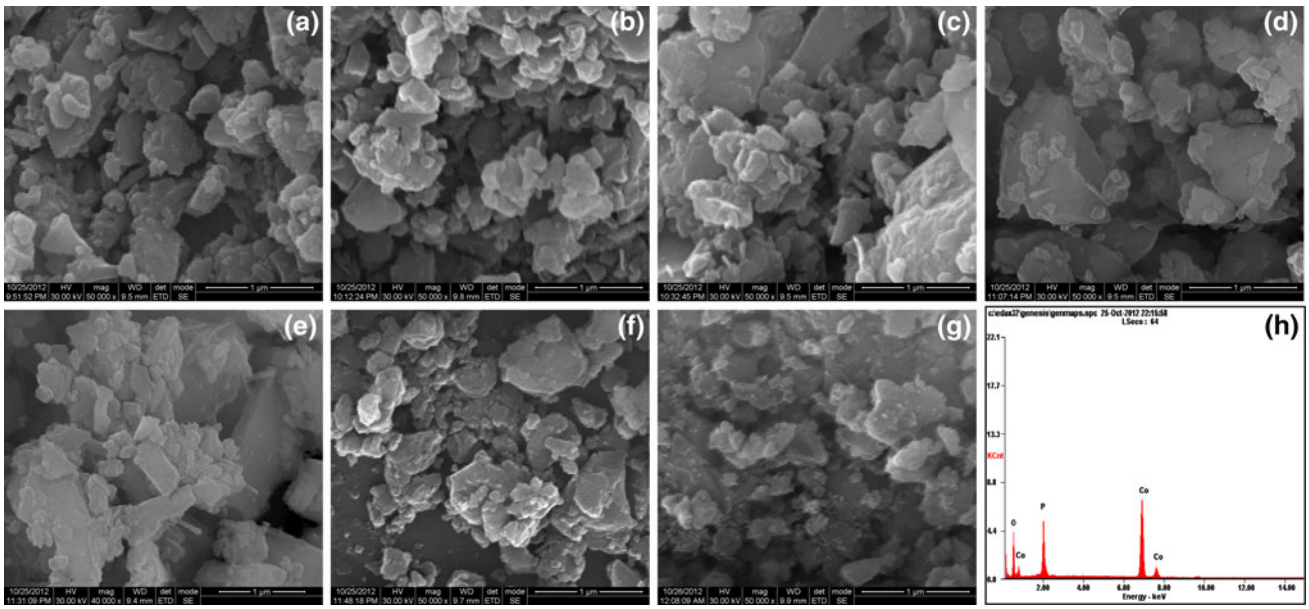

Fig. 3 HRSEM image of **a** $LiCoPO_4$, **b** $LiCo_{0.98}V_{0.02}PO_4$ **c** $LiCo_{0.96}V_{0.04}PO_4$, **d** $LiCo_{0.94}V_{0.06}PO_4$, **e** $LiCoP_{0.98}V_{0.02}O_4$, **f** $LiCoP_{0.96}V_{0.04}O_4$ and **g** $LiCoP_{0.94}V_{0.06}O_4$ **h** EDAX spectra of $LiCoPO_4$

(PO_4^{3-}) which is made of strong covalent bonds that provides stable structure to the compound. The band (ν_1) between 900–1,100 cm^{-1} and bands (ν_2) 400–700 cm^{-1} attributes to the symmetric stretching and bending vibration of the tetrahedral anion, respectively. Similarly, the bands between (ν_3) 1,050–1,150 cm^{-1} and (ν_4) 647 cm^{-1} corresponds to the asymmetric stretching and bending mode of the tetrahedral anion, and the other weak bands in the region of 500–590 cm^{-1} attributes to the stretching modes of CoO_6 [28].

The fundamental vibration of PO_4^{3-} in pristine $LiCoPO_4$ is observed in the range of 970 cm^{-1} matches well with the reported values and for the doped material in cobalt site ($LiCo_{1-x}V_xPO_4$) the band is observed in the range of 967–970 cm^{-1}. Similar type of results was observed from the previous study in the case of Ni ion substitution at Co^{2+} site, since the dopant effect is only predominant at high concentration [25]. But in the case of $LiCoP_{1-x}V_xO_4$ the strong stretching band at about 970 cm^{-1} gets broaden which indicates that the large ionic radii vanadium slightly influence the local structure of the polyanion network of the compound. Thus the difference in the wave number shift of two doped materials reveals that the dopant vanadium exactly occupy the corresponding Co^{2+} and P^{5+} site of $LiCo_{1-x}V_xPO_4$ and $LiCoP_{1-x}V_xO_4$ strengthening the coordination between the atoms.

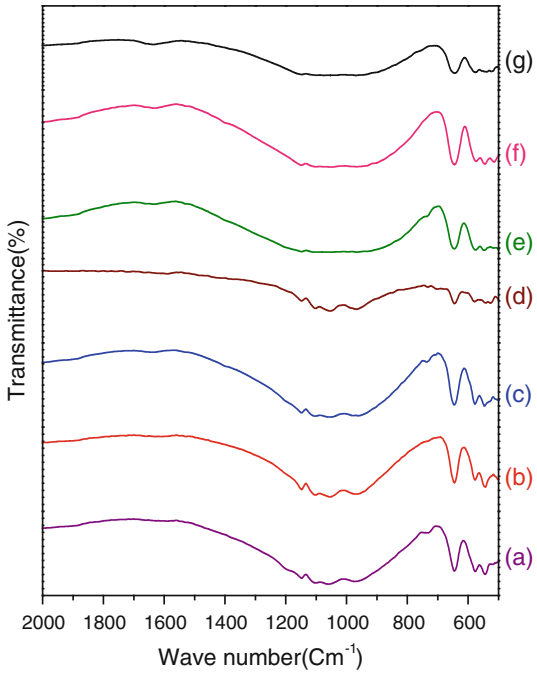

Fig. 4 FTIR spectra of (*a*) $LiCoPO_4$, (*b*) $LiCo_{0.98}V_{0.02}PO_4$, (*c*) $LiCo_{0.96}V_{0.04}PO_4$, (*d*) $LiCo_{0.94}V_{0.06}PO_4$, (*e*) $LiCoP_{0.98}V_{0.02}O_4$, (*f*) $LiCoP_{0.96}V_{0.04}O_4$ and (*g*) $LiCoP_{0.94}V_{0.06}O_4$

3.5 Raman spectroscopy

Raman spectroscopy is a powerful technique in the structural analysis of complex compound. Figure 5 shows the representative Raman spectrum of pristine and vanadium doped $LiCoPO_4$ It shows that there was a strong band at around 946.8 cm^{-1} and other weak signals were obtained in the ranges of 578.3 and 242.18 cm^{-1} confirming the synthesized material to be $LiCoPO_4$ which was already confirmed by the FTIR analysis. Generally, the Raman

spectrum is divided into two regions below and above 400 cm^{-1}. The bands obtained above 400 cm^{-1} corresponds to the strong bands due to the internal vibration modes whereas the bands below 400 cm^{-1} corresponds to the external lattice modes. The internal modes splits up into four fundamental bands ($\nu_1 - \nu_3$) at 950, 1,090 of P–O that corresponds to the symmetric and asymmetric stretching and bands at ($\nu_2 - \nu_4$) 590, 448 corresponding to the O–P–O symmetric and asymmetric bending [29]. In the present study, the strong band obtained in the internal vibrational mode, A_g mode of covalent complex PO_4^{3-}, for $LiCoPO_4$ is 948.8 cm^{-1} which is well matched with the reported values (950–960 cm^{-1}) [29, 30]. The other Raman signals in the low frequency modes are weak in $LiCoPO_4$. A similar result was also obtained for the doped samples. However, for the doped samples the band around 946.8 cm^{-1} is slightly changed to 943–947 cm^{-1}. The change in wave number peak intensity in both cases of doped materials reveals that the dopant is exactly occupying the corresponding host lattice. The peak intensity and wave number shift is lowered in the case of dopant in the Co^{2+} site whereas in the case of P^{5+} it was higher, which revealed that the presence of dopant strengthened the coordination (bond length) of the compound as already seen from FTIR analysis. However, the addition of dopant does not affect the structure more significantly. This reveals that the $LiCoPO_4$ is dominated by the PO_4 network. Thus the Raman and the FTIR analysis shows more or less same range in the fundamental vibrational mode of PO_4 network which confirmed the materials to be $LiCoPO_4$, $LiCo_{1-x}V_xPO_4$ and $LiCoP_{1-x}V_xO_4$.

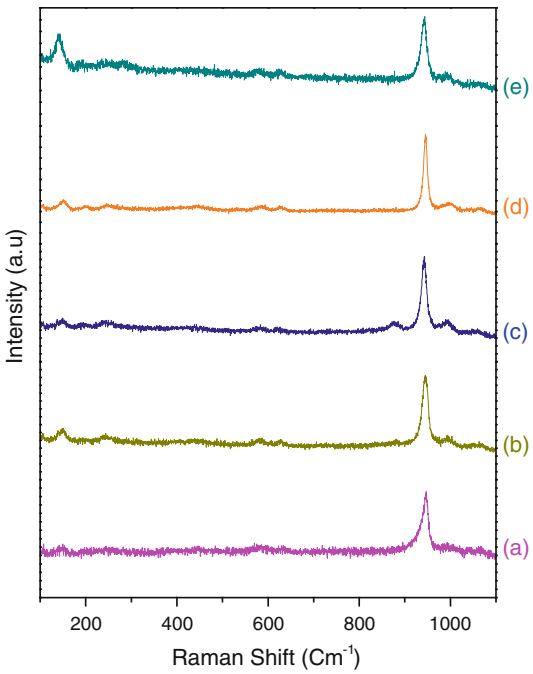

Fig. 5 Raman spectrum of $LiCoPO_4$ (*a*) $LiCoPO_4$, (*b*) $LiCo_{0.98}V_{0.02}PO_4$, (*c*) $LiCo_{0.96}V_{0.04}PO_4$, (*d*) $LiCoP_{0.98}V_{0.02}O_4$ and (*e*) $LiCoP_{0.96}V_{0.04}O_4$

3.6 X-ray photoelectron spectroscopy (XPS) analysis

The XPS analysis was carried out in order to study the oxidation state of each element in the compound. Figure 6a–e shows the O 1s, P 2p, Co 2p, V 2p, C 1s high resolution XPS spectra of pristine $LiCoPO_4$, $LiCo_{0.94}V_{0.06}PO_4$ & $LiCoP_{0.94}V_{0.06}O_4$. The obtained spectra for pristine $LiCoPO_4$ were in match with the reported data [11]. The O 1s peak of $LiCoPO_4$ shows a single peak with binding energy of 531.33 eV which indicates the oxidation state of oxygen in the compound to be divalent. The C 1s carbon residues present as a result of combustion product shows a peak corresponding to binding energy value of 284.52 eV. Similarly, the P 2p & Co 2p peaks of pristine $LiCoPO_4$ were obtained at 133.5 and 781 eV corresponds to the P^{5+} & Co^{2+} state [31]. Also, there is no sign of vanadium peaks observed for the pristine $LiCoPO_4$ samples. It is also to be noted that, the doped $LiCo_{0.94}V_{0.06}PO_4$ & $LiCoP_{0.94}V_{0.06}O_4$ materials possess a similar kind of spectra that of the parent with slight variation in their binding energy values. The V 2p peaks could be observed for the doped $LiCo_{0.94}V_{0.06}PO_4$ & $LiCoP_{0.94}V_{0.06}O_4$ materials in the range of 520 eV. The C1s peak for $LiCo_{0.94}V_{0.06}PO_4$ & $LiCoP_{0.94}V_{0.06}O_4$ materials are at 284.49 and 284.508 eV, respectively. The O 1s peak of two doped samples $LiCo_{0.94}V_{0.06}PO_4$ & $LiCoP_{0.94}V_{0.06}O_4$ were obtained at 532.3 and 531.39 eV and the peaks for Co 2p were obtained at 782.7 and 781.3 eV, respectively. Also the peaks for P 2p were observed at 134.857 eV and 133.5 eV for $LiCo_{0.94}V_{0.06}PO_4$ and $LiCoP_{0.94}V_{0.06}O_4$. This slight deviation could be attributed to the structural variation caused as a result of dopant addition on Co^{2+} & P^{5+} site of the $LiCoPO_4$ material. The above observations revealed that the addition of vanadium affect the local structure of the compound since there is shift in the binding energy values of $LiCo_{0.94}V_{0.06}PO_4$ which attributes to the change in the M–O bonding in the compound similar effects were obtained in the literature [21]. Evidently in the case of dopant, there is no appreciable change in the structure for phosphate site doped materials when compared to the metal site (Co^{2+}) doped compounds. So the structural variation is prominent in metal site (Co^{2+}) than the phosphate site (P^{5+}) doped samples. This is an additional proof for the structural variation of metal site doped samples. As it is already seen in the XRD results, the lattice parameter values get changed only at high concentration of vanadium (0.06). These results enumerate the fact that the vanadium doping at the metal site would shows a considerable change in the electrochemical performance.

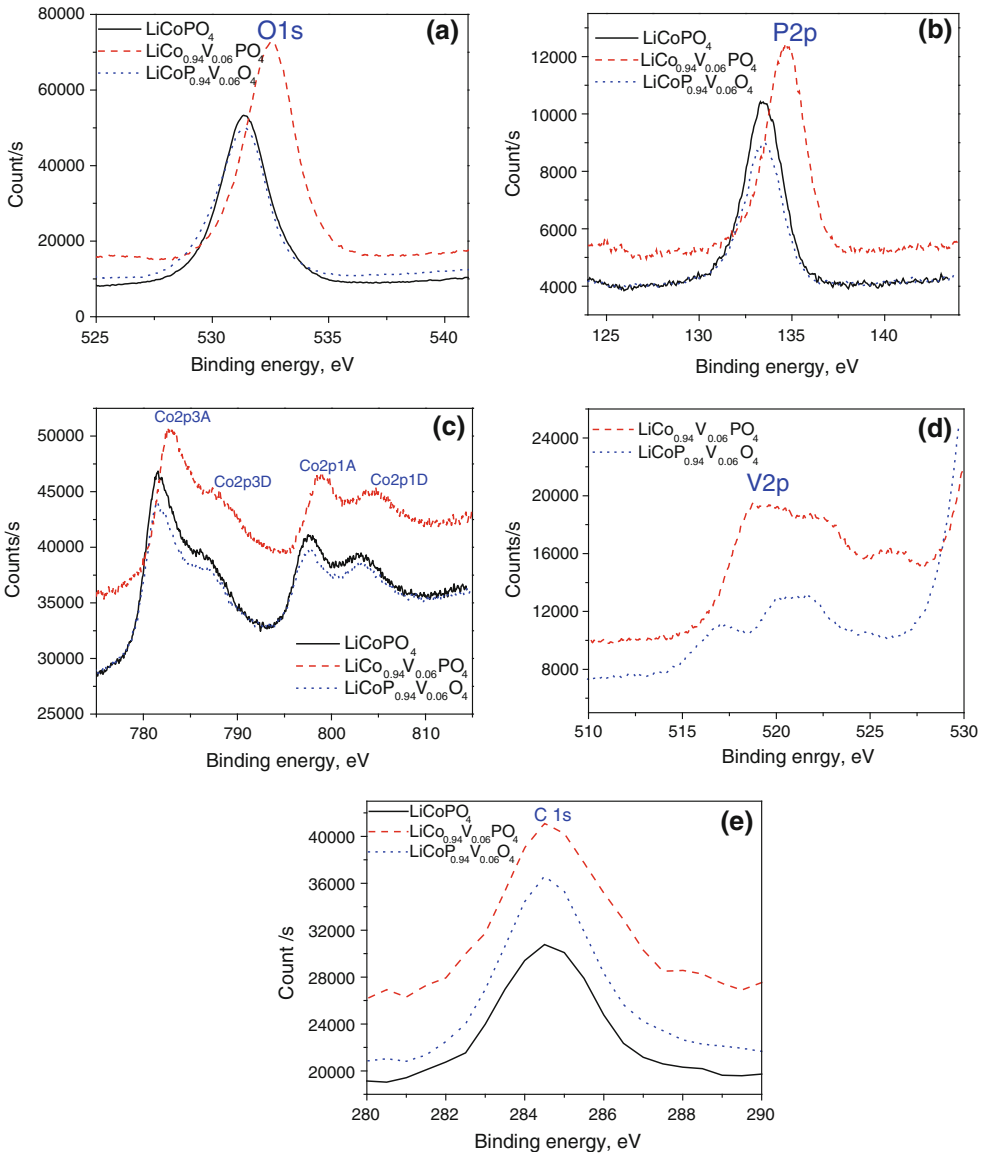

Fig. 6 High resolution XPS Spectra of **a** O 1s, **b** P 2p, **c** Co 2p, **d** V 2p, **e** C 1s for pristine and doped samples $LiCoPO_4$

3.7 Electrochemical performance

3.7.1 Electrochemical impedance spectroscopy

Figure 7a, b shows the Nyquist plots of pristine $LiCoPO_4$, $LiCo_{1-x}V_xPO_4$ and $LiCoP_{1-x}V_xO_4$ (x = 0.0, 0.02, 0.04, 0.06) materials. The impedance spectrum possesses a single semicircle with a straight line that infers the presence of charge transfer conduction behavior in the materials. The semi circle at high frequency region was attributed to the solution resistance R_s, mid frequency semicircle corresponds to the charge transfer resistance R_{ct} and the tail like line at low frequency region corresponds to the Warburg diffusion of lithium ions. The impedance values were taken from the fitted curves with the equivalent circuit model (given as an inset in Fig. 7 b) is given in Table 2. It was observed that the resistance gets increased in the doped samples in both the cases ($LiCo_{1-x}V_xPO_4$ and $LiCoP_{1-x}V_xO_4$) which reveal that the conductivity is not enhanced by the addition of dopant. However it was also noted that in both cases of $LiCo_{1-x}V_xPO_4$ and $LiCoP_{1-x}V_xO_4$, the impedance value of doped samples get reduced at high concentration (0.06) compared to other concentrations. The significant structural variation could be observed only at high concentration (0.06) of dopant addition as revealed from the XRD & XPS analysis. Still the impedance is high compared to pristine $LiCoPO_4$; the reason being the decrease in the cell volume of doped samples as seen from the XRD analysis. This reduction in the cell volume restricts the movement of carriers due to lattice contraction which attributes to the low ionic radii of the vanadium compared to cobalt [23] leading to poor conductivity. In the case of dopant in the phosphate site, similar behavior is observed

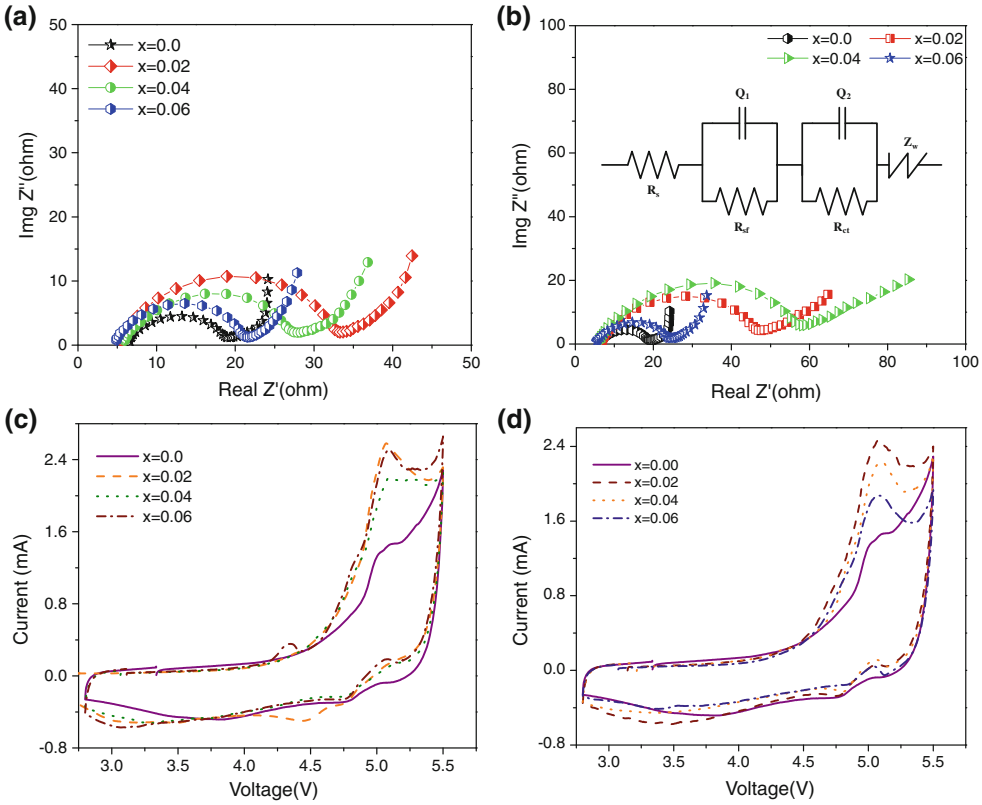

Fig. 7 Nyquist plot of **a** $LiCo_{1-x}V_x\ PO_4$ & **b** $LiCoP_{1-x}V_xO_4$ (*inset* equivalent circuit model), CV curves of **c** $LiCo_{1-x}V_xPO_4$ & **d** $LiCoP_{1-x}V_xO_4$

because the vanadium doping in phosphate site just slightly influence the local structure of phosphate ion but it is not that much measurable, and the strong covalent nature of PO_4 molecule is not disturbed by any addition of dopant as already seen in FTIR and Raman analysis. Since the XPS results also substantiates the structural variation is prominent at the Co^{2+} site doped samples at high concentration (0.06) than the P^{5+} doped samples. Therefore, in the present study the electrical conductivity reflects the structural characteristics and morphology of the obtained materials. Generally, it is known that the strong covalent bond of PO_4^- formed their valence and conduction bands far from the Fermi level because of the closed shell configuration. This makes the valence electrons of transition metals to be an isolated one leading to poor electrical conduction [32]. There is also no appreciable structural or morphological changes occurred to enhance the conductivity by the effect of V^{5+} doping. The theoretical approaches predict that the selectivity of dopant is related to substitution energy of the dopant. Those predictions suggest that the doping of cation site is favored only for the isovalent substitution (M^{2+}) which is having low substitution energy. In addition, the dopants like supervalent elements (M^{5+}) are unstable in the crystal lattice of the host material [33]. The presence of supervalent dopant in the host lattice creates a non stoichiometric and instability which leads to controversial role in electrochemical enhancement and remains uncertain [34]. Therefore, from the EIS studies it is clear that the pure $LiCoPO_4$ and vanadium doped samples possess an electrochemical behavior but the electrical conduction is not in an appreciable manner. This suggests that the irregular morphology of the present materials greatly affected the conduction property.

3.7.2 *Cyclic voltammetry*

The CV of pristine $LiCoPO_4$, $LiCo_{1-x}V_xPO_4$ and $LiCoP_{1-x}V_xO_4$ recorded at a scan rate of 0.2 mVs^{-1} in the potential range of 2.8–5.5 V are shown in Fig. 7c, d. The CV curves indicated that all the cathode materials show a good reversibility. For the pristine $LiCoPO_4$, the oxidation and reduction peaks appeared at 5.02 and 4.78 V was attributed to the Li^+ deintercalation and intercalation during the electrochemical process. The peak potentials obtained in the present work matches well with the reported values. A similar type of behavior is observed for the V^{5+} doped materials [17, 19]. Interestingly, the doped materials showed a well defined redox peaks in the potential range of 5.07–5.09 and 4.7–4.8 V. In addition, the current rates of the doped materials get increased compared to pristine $LiCoPO_4$ which implies that the electrochemical kinetic behavior is enhanced for both types ($LiCo_{1-x}V_xPO_4$ & $LiCoP_{1-x}V_xO_4$) of doped materials especially in the case of dopant in Co^{2+} site at the

Table 2 Electrochemical parameters

Compounds	EIS datas		CV datas		
	Solution resistance R_s (ohm)	Charge transfer resistance R_{ct} (ohm)	Anodic peak potential (V)	Cathodic peak potential (V)	Potential difference (V)
$LiCoPO_4$	6.19	13.02	5.02	4.75	0.27
$LiCo_{0.98}V_{0.02}PO_4$	5.19	27.32	5.07	4.74	0.33
$LiCo_{0.96}V_{0.04}PO_4$	5.62	21.88	5.09	5.25	0.16
$LiCo_{0.94}V_{0.06}PO_4$	4.48	16.38	5.08	5.15	0.07
$LiCoP_{0.98}V_{0.02}O_4$	6.51	41.66	5.07	5.15	0.06
$LiCoP_{0.96}V_{0.04}O_4$	5.68	54.25	5.09	5.14	0.05
$LiCoP_{0.94}V_{0.06}O_4$	5.18	19.23	5.07	5.12	0.04

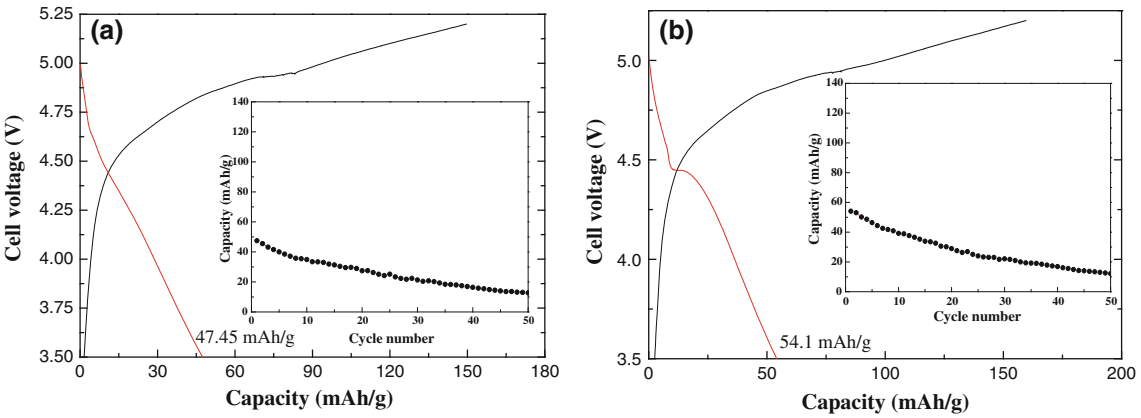

Fig. 8 Charge-discharge curve & cycle number plot of **a** $LiCoPO_4$ **b** $LiCo_{0.98}V_{0.02}PO_4$

concentration of 0.06, since the impedance value of $LiCo_{0.94}V_{0.06}PO_4$ is less compared to other concentrations. Further, the potential difference between the anodic and cathodic peak shown in Table 2 shows that electrode polarization of doped materials in both cases is high compared to pristine $LiCoPO_4$ but it get reduced for the doped material at high concentration (0.06). Since the XPS results revealed that the structural variation is well observed for the Co^{2+} metal site doped materials at high concentration (0.06). Hence, the doped samples might show a good electrochemical behavior. But the appearance of dual reduction peak in the doped materials may be due to the presence of inactive species during the reversible cycle which may leads to poor performance and irreversibility [35]. These effects will limit the Li^+ ion diffusion during the electrochemical performance. Now it is well clear that the morphology of the present material affects the electrochemical behavior too. The above results conclude that the doped materials show an electrochemical reversible performance for high dopant concentration samples but it was hindered by the inactive phases.

3.7.3 Charge–discharge analysis

The charge–discharge studies were conducted for the pristine and vanadium doped materials ($LiCo_{1-x}V_xPO_4$ and $LiCoP_{1-x}V_xO_4$ x = 0, 0.02, 0.04, 0.06) between 3.5 and 5.2 V versus Li at room temperature. The representative charge–discharge curves and the corresponding cycle number plots for the pristine and vanadium doped $LiCoPO_4$ is shown in Fig. 8a, b. The charging capacity of pristine $LiCoPO_4$ is 150 mAh g^{-1} and the obtained discharge capacity is 47.45 mAh g^{-1} with the voltage plateau close to 4.8 V but the voltage plateau was not distinct which clearly reveals the presence of voltage drop due to electrode polarization and poor electrode kinetics which is already revealed from CV analysis. Similar results were reported in recent years [36, 37]. The charging capacity of doped samples in the Co site were 160, 140 and 130 mAh g^{-1} and the corresponding discharge capacity were 54.1, 43.55 and 38.9 mAh g^{-1}. Similarly, the charge–discharge capacity of doped materials in the P site are also

low (120, 110, 80 mAh g^{-1} and 32.9, 32.9, 21 mAh g^{-1}) compared to the previous one. The cycling performance of pristine and all the doped materials of $LiCoPO_4$ reveal that the capacity is gradually decreased and the retention was only 20 % after 50 cycles. This poor electrochemical performance and capacity fading is attributed to the poor electrical conductivity of the materials and the presence of inactive species during cycling which is greatly driven by the morphology and particle size, since the obtained materials are in sub micron size. Additionally, the charge–discharge studies revealed the potential instability during electrochemical performance which may be due to the electrolyte decomposition and corrosion of current collector at the high potential close to 5.1 V [35] which can be reduced by carbon coating. But the discharge capacity and performance of the present material is still better than the previous reported values like 14 and 37 mAh g^{-1} [13, 37] which was attributed to the larger particle size leading to poor rate performance.

It is cleared from the above results that the pristine and vanadium doped materials ($LiCo_{1-x}V_xPO_4$ & $LiCoP_{1-x}V_xO_4$ x = 0.00, 0.02, 0.04, 0.06) possess a good thermal and structural stability which are a favorable properties for a good electrochemical system. However, the poor electrical conduction of the present materials is a main drawback which is due to the irregular morphology and large size of the particles. The CV results gave a hope that it would be suitable materials if the above drawbacks could be rectified in the future. Therefore, some remedial measures like particle size reduction and carbon coating along with suitable doping can be taken to improve the conductivity thereby reaching a better performance. In addition, some of the facts from the obtained results are unclear that is the doping in phosphate site does not make any significant changes in the structure. But, the presence of vanadium is somehow affecting the molecular vibration which is shown from FTIR, Raman & XPS analysis. The presence of inactive phases of doped materials from CV results was unclear. The EIS and CV results show a similar behavior in both cases but among them doping in the Co site shows a good behavior when compared to the phosphate site doped material. The EIS results revealed that impedance get reduced for doped materials at high concentration (0.06). Further the charge–discharge studies showed a poor electrochemical performance and capacity fading over many cycles which strongly recommends the importance of reduction of particle size and the morphology which are the main driving force of electrochemical performance as reported by all the researchers. Since, it is a preliminary study on the effect of vanadium doing on the structure and electrochemical performance without carbon coating, the results still gave us a hope to rectify the poor performance in the future by carbon coating and particle size reduction.

4 Conclusion

$LiCoPO_4$, $LiCo_{1-x}V_xPO_4$ & $LiCoP_{1-x}V_xO_4$ (x = 0.02, 0.04, 0.06) were successfully prepared by means of combustion method. The X-ray diffraction patterns of prepared $LiCoPO_4$ and vanadium doped samples confirmed its pure phase olivine structure. The structural changes on the addition of dopant were revealed from FTIR and Raman analysis since there was a shift in absorbed bands of doped samples. The SEM images showed irregular shaped and large size particles of the samples. The XPS results showed the structural variation of doped samples at high concentration. The EIS measurements demonstrated the presence of charge transfer conduction phenomenon of the samples; however, the conductivity is not enhanced on the addition of dopant which is mainly due to the irregular morphology. The CV plots of all the samples illustrated that the present materials possess a good electrochemical reversibility with a redox peaks at 4.7–5 V and the charge–discharge studies revealed a poor performance over many cycles but it can be rectified. Therefore, the above results suggest that the vanadium doped samples could be used as a cathode material for Li –ion batteries by serious consideration on control of morphology.

References

1. Whittingham Stanley M (2004) Chem Rev 104:4271–4301
2. Fergus WJ (2010) J Power Sources 195:939–954
3. Palacin RM (2009) Chem Soc Rev 38:2565–2575
4. Padhi AK, Nanjundaswamy KS, Goodenough JB (1997) J Electrochem Soc 144:1187–1194
5. Martha SK, Grinbat J, Haik O, Zinigrad E, Drezen J, Miners JH, Exnar J, Kay A, Markovsky B, Aurbach D (2009) Angew Chem Int Ed 48:8559–8563
6. Martha SK, Markovsky B, Grinbat J, Gofer Y, Haik O, Zinigrad E, Aurbach D, Drezen J, Wang D, Denghenghi G, Exnar I (2009) J Electrochem Soc 156:A541–A552
7. Okada S, Sawa S, Egashira M, Yamaki J, Tabuchi M, Kageyama H, Konishi T, Yoshino A (2001) J Power Sources 97–98:430–432
8. Ruffo R, Huggins RA, Mari CM, Piana M, Weppner W (2005) Ionics 11:213–219
9. Bramnik NN, Bramnik Kirill G, Buhrmester T, Baehtz C, Ehrenberg H, Fuess H (2004) J Solid State Electrochem 8:558–564
10. Bramnik NN, Bramnik Kirill G, Baehtz C, Ehrenberg H (2005) J Power Sources 145:74–81
11. Long T, Luo Z, Liu H, Yu Y (2010) J Alloys Compd 502: 407–410
12. Kalyani P, Kalaselvi N, Muniyandi N (2002) Mater Chem Phys 77:662–668
13. Yujuan Z, Suijun W, Chunsong Z, Dingguo X (2009) Rare Met 28:117–121
14. Rabanal ME, Gutierrez MC, Alvarado GF, Gonzalo EC, Dompablo A (2006) J Power Sources 160:523–528
15. Gangulibabu D, Bhuvaneswari N, Kalaiselvi N, Jayaprakash N, Periasamy P (2009) J Sol-Gel Sci Technol 49:137–144
16. Jin B, Gu H-B, Kim K-W (2008) J Solid State Electrochem 12:105–111

17. Li HH, Jin J, Wei JP, Zhou Z, Yan J (2009) Electrochem Commun 11:95–98
18. Doan Long N, Taniguchi I (2011) J Power Sources 196: 5679–5684
19. Han Wook D, Kang Mook Y, Yin ZR, Song MS, Kwon SK (2009) Electrochem Commun 11:137–140
20. Wang F, Yang J, Nuli Y, Wang J (2010) J Power Sources 195: 6884–6887
21. Wang D, Wang Z, Huang X, Chen L (2005) J Power Sources 146: 580–583
22. Li M (2012) Ionics 18:507–513
23. Satya Kishore MVVM, Varadaraju UV (2005) Mater Res Bull 40:1705–1712
24. Allen JL, Jow TR, Wolfenstine J (2011) J Power Sources 196:8656–8661
25. Shanmugaraj D, Murugan R (2004) Ionics 10:88–92
26. Jang IC, Son CG, Yang SMG, Lee JW, Cho AR, Aravindan V, Park GJ, Kang KS, Kim WS, Cho WI, Lee YS, Ait Salah A, Gendron F, Morhange JF, Mauger A, Ramana CV (2011) J Mater Chem 21:6510–6514
27. Wolfenstine J (2006) J Power Sources 158:1431–1435
28. Poovizhi PN, Selladurai S (2011) Ionics 17:13–19
29. Julien CM, Ait Salah A, Gendron F, Morhange JF, Mauger A, Ramana CV (2006) Scripta Mater 55:1179–1182
30. Markevich E, Sharabi R, Haik O, Borgel V, Salitra G, Aurbach D, Semrau G, Schmidt MA, Schall N, Stinner C (2011) J Power Sources 196:6433–6439
31. Nithya C, Thirunakaran R, Sivashanmugam A, Gopukumar S (2012) Chem Asian J 7:163–168
32. Nakayama M, Goto S, Uchimoto Y, Miyanaga M, Wakihara Y, Kitajima T, Watanable I (2005) J Phys Chem B 109:11197–11203
33. Fisher CAJ, Hart Prieto VM, Islam MS (2008) Chem Mater 20:5907–5915
34. Wagemaker M, Ellis LB, Hecht DL, Mulder FM, Nazar LF (2008) Chem Mater 20:6313–6315
35. Jang IC, Lim HH, Lee SB, Karthikeyan K, Aravindan V, Kang KS, Yoon WS, Cho WI, Lee YS (2010) J Alloys Compd 497:321–324
36. Prabhu M, Selvasekarapandian S, Reddy MV, Chowdari BVR (2012) J Solid State Electrochem 16:1833–1839
37. Dimesso L, Jacke S, Spanheimer C, Jaegermann W (2012) J Solid State Electrochem 16:911–919